Charged-current neutrino-nucleus scattering off ^{127}I and ^{133}Cs

Matti Hellgren [*]
Department of Physics, University of Jyväskylä, P.O. Box 35, FI-40014, Finland

Jouni Suhonen [†]
Department of Physics, University of Jyväskylä, P.O. Box 35, FI-40014, Finland
and International Centre for Advanced Training and Research in Physics (CIFRA), P.O. Box MG12, 077125 Bucharest-Magurele, Romania

(Received 18 September 2023; accepted 6 February 2024; published 11 March 2024)

Calculations of (anti)neutrino-nucleus scattering cross sections are vital since experimental results for these cross sections for terrestrial-based (anti)neutrino sources in the low-to-intermediate energy ranges are exceedingly rare. A recent measurement of the scattering of stopped-pion neutrinos off ^{127}I by the COHERENT Collaboration yielded a cross section that was only 41% of the expected theoretical prediction. Inspired by this, we have computed the cross sections for (anti)neutrino scatterings off ^{127}I and ^{133}Cs by considering also the effect of the quenching of the weak axial coupling $g_{\rm A}$ on the results. Two quenching schemes, a conservative and a radical estimate, were considered. The cross sections as functions of the neutrino energy are presented along with folded cross sections for stopped-pion and supernova (anti)neutrino spectra. The nuclear model used was the microscopic quasiparticle-phonon model based on large single-particle model spaces and realistic *G*-matrix-based effective two-body interactions. The obtained inclusive cross sections for stopped-pion neutrino scattering off ^{127}I are in good agreement with the experimental results. The results indicate that discrepancy between the experimental and theoretical results could be at least partly explained by the quenching of $g_{\rm A}$.

DOI: 10.1103/PhysRevC.109.035802

I. INTRODUCTION

The field of neutrino-nucleus interactions has generated a substantial amount of interest in recent decades. Large national and multinational experimental collaborations such as Super-Kamiokande [1], Sudbury Neutrino Observatory (SNO) [2], Ice Cube [3], and the COHERENT experiment [4] have yielded a number of highly notable results including experimental evidence for neutrino oscillations [5,6] and detection of the coherent elastic neutrino-nucleus scattering (CEνNS) process [7]. In addition to the many currently running neutrino experiments, a number of large-scale next generation detectors such as the Jiangmen Underground Neutrino Observatory (JUNO) [8], the European Spallation Source neutrino Super Beam (ESSνSB) [9], and the Accelerator Neutrino Neutron Interaction Experiment (ANNIE) [10] are under construction or at planning stage. As a result, interest in the field is expected to only increase in the near future.

Despite a growing number of neutrino experiments, there currently exists experimental results of terrestrial-based neutrino scattering for only seven nuclear targets in the low-intermediate energy range [11–13]. A recent measurement of the charged-current stopped-pion electron neutrino scattering cross section off ^{127}I by the COHERENT Collaboration [14] is therefore of particular interest. The experimental result for the cross section of the inclusive reaction was found to be only about 41% of an expected theoretical estimate obtained by using the Model of Argon Reaction Low Energy Yields (MARLEY), a Monte Carlo event generator for neutrino-nucleus interactions [15]. There is no immediately obvious likely cause for this apparent disagreement that would explain it completely. One factor that could explain the discrepancy is the effective (quenched) value used for the weak axial-vector coupling $g_{\rm A}$. In this paper we explore this possibility in detail.

The use of iodine in neutrino and dark matter detectors has been and remains common in the past and present experiments. It is typically utilized in the form of thallium-doped cesium-iodide crystals CsI [Tl], as in the KIMS experiment [16], sodium-doped cesium-iodide crystals CsI[Na], as in the COHERENT experiment [7], or thallium-doped sodium-iodide, as in DM-Ice [17], PICO-LON [18], and ANAIS [19]. As cesium is often present in the detectors with iodine, it is natural to consider both ^{127}I and ^{133}Cs and their neutrino scattering properties instead of just one of them. The two nuclei have similar mass numbers and nuclear shell model shell occupations, so it is reasonable to utilize the same nuclear model and valence space for modeling both of them.

The primary goal of this paper is to compute accurate and realistic charged-current (anti)neutrino scattering cross sections off ^{127}I and ^{133}Cs and compare the them to the recent experimental results. Special care is taken regarding

[*]majokahe@jyu.fi
[†]jouni.t.suhonen@jyu.fi

the choice of the effective value of $g_{\rm A}$ (or $g_{\rm A,eff}$) used in the calculations. In particular, we obtain separate values of $g_{\rm A,eff}$ for the two nuclear targets based on a systematic analysis of allowed β-decay half-lives of nuclei in a wide range of mass numbers as a conservative estimate for the quenching. We also consider a more radical approach to quenching based on rough estimates of $g_{\rm A,eff}$ values obtained from forbidden decays. The nuclear model we use in modeling the initial and final state nuclear wave functions is the microscopic quasiparticle-phonon model (MQPM).

Several prior theoretical studies into the charged-current neutrino scattering cross section off ^{127}I exist, with varying results [20–26]. Much of this research is quite old (at least 15 to over 30 years) and was thus conducted with, by modern standards, relatively limited available computational power. ^{127}I and ^{133}Cs are also open-shell nuclei with large numbers of valence nucleons so shell-model calculations were prohibitively expensive for obtaining spectra of states up to the energies required for a realistic description of intermediate-energy (anti)neutrino (such as supernova or stopped-pion) scattering. Older scattering cross section calculations thus either had to rely on somewhat drastic simplifying approximations to the nuclear models used [21,22], or utilized methods that avoided the construction of explicit final states altogether, such as the closure approximation [27,28] and Fermi gas models [29,30]. It is also worth noting that recent research for low-energy neutrino-nucleus charged-current scattering off ^{127}I in the form of solar neutrino scattering exists [31–33].

The chosen value of $g_{\rm A,eff}$ also varies in the previous research. The effective value of the weak axial-vector coupling inside nuclear matter has been long known to differ from the corresponding free value in the case of nuclear β decay [34,35]. As accurate (anti)neutrino-nucleus scattering cross-section measurements are considerably more difficult than measurements of the half-lives of typical β decays, studies into the quenching of $g_{\rm A}$ in β decays provides a valuable way of estimating the quenching in (anti)neutrino-nucleus scattering and other weak nuclear processes. New systematic studies into the quenching of $g_{\rm A}$ in various β and $\beta\beta$ decays have been conducted during the last decade [36]. The findings in the mentioned studies can be applied to (anti)neutrino-nucleus scattering calculations in an attempt to choose the value of $g_{\rm A,eff}$ more accurately in order to obtain more accurate results for the cross sections, which is precisely the goal of this paper.

This paper is organized as follows: In Sec. II we briefly review the theory of semileptonic nuclear processes with special emphasis on the emergence and role of the weak axial-vector coupling $g_{\rm A}$ and the procedure by which its effective values used in the scattering calculations were obtained. We also discuss the nuclear many-body framework used in the construction of the nuclear states, presenting also the obtained theoretical spectra for the nuclei of interest. In Sec. III we present the results for the scattering cross sections as functions of the energy of the incoming (anti)neutrino, along with the folded cross sections for stopped-pion and supernova (anti)neutrinos. The results of the two different quenching schemes are also compared to the experimental results for the scattering off ^{127}I. Finally, in Sec. IV we discuss the conclusions that can be drawn from the obtained results themselves and their comparisons to corresponding experimental results.

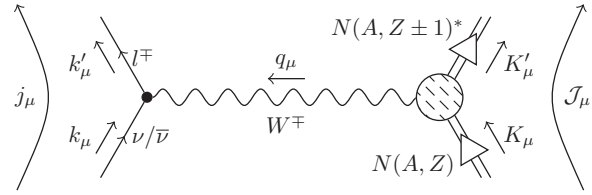

FIG. 1. Feynman diagram illustrating the reaction where an incoming (anti)neutrino $(\overline{\nu})\nu$ scatters off an atomic nucleus $N(A,Z)$ via the exchange of a charged $W^\mp$ boson, producing the final state lepton $l^\mp$ and the daughter nucleus $N(A,Z\pm1)^*$, which may be in an excited state. The four-momenta of the lepton and nucleus prior to the scattering are denoted by k_μ and K_μ, and after the scattering by k'_μ and K'_μ, respectively. The transferred 4-momentum is denoted by $q_\mu = k'_\mu - k_\mu = K_\mu - K'_\mu$.

II. THEORETICAL FORMALISM

A. Neutrino-nucleus scattering

A charged-current neutrino-nucleus scattering reaction can be expressed as

$$\nu/\overline{\nu} + N(A,Z) \longrightarrow l^\mp + N(A,Z\pm1)^*, \qquad (1)$$

where $(\overline{\nu})$ ν denotes an initial state (anti)neutrino, (l^+) l^- a final state (anti)lepton, and $N(A,Z)$ and $N(A,Z\pm1)^*$ the initial and final state nuclei. This process proceeds via an exchange of the charged vector boson $W^\mp$, and is illustrated in Fig 1. In addition to the possibility of the reaction of leaving the final state nucleus in an excited state [denoted by $*$ in Eq. (1) and suppressed hereafter, unless stated otherwise], the final state nuclear species is also different from that of the initial state nucleus, and as a result these reactions can have a threshold energy. The relevant reactions considered in this paper are, with the threshold energies (in keV) in parentheses, the following [37]:

$$\begin{aligned}
\nu_e + {}^{127}\mathrm{I} &\longrightarrow e^- + {}^{127}\mathrm{Xe} \quad (662\pm6),\\
\overline{\nu}_e + {}^{127}\mathrm{I} &\longrightarrow e^+ + {}^{127}\mathrm{Te} \quad (1725\pm5),\\
\nu_e + {}^{133}\mathrm{Cs} &\longrightarrow e^- + {}^{133}\mathrm{Ba} \quad (517\pm2),\\
\overline{\nu}_e + {}^{133}\mathrm{Cs} &\longrightarrow e^+ + {}^{133}\mathrm{Xe} \quad (1449\pm3),
\end{aligned} \qquad (2)$$

where the initial nuclei are in their ground states. These reactions are also illustrated in Fig. 2. The scatterings of μ and τ neutrinos have threshold energies of $\gtrsim$106 and $\gtrsim$1777 MeV (the masses of the μ and τ leptons [38]), far beyond the relevant energy ranges of typical astrophysical neutrinos ($\lesssim$ 18 MeV for solar neutrinos and $\lesssim$ 80 MeV for supernova neutrinos [39]), and we will thus not consider these reactions here.

To compute the scattering cross sections we have utilized the Donnelly-Walecka formalism [40,41] for semileptonic nuclear processes. The scattering process of Fig. 1 can be treated as a more simple pointlike current-current interaction between

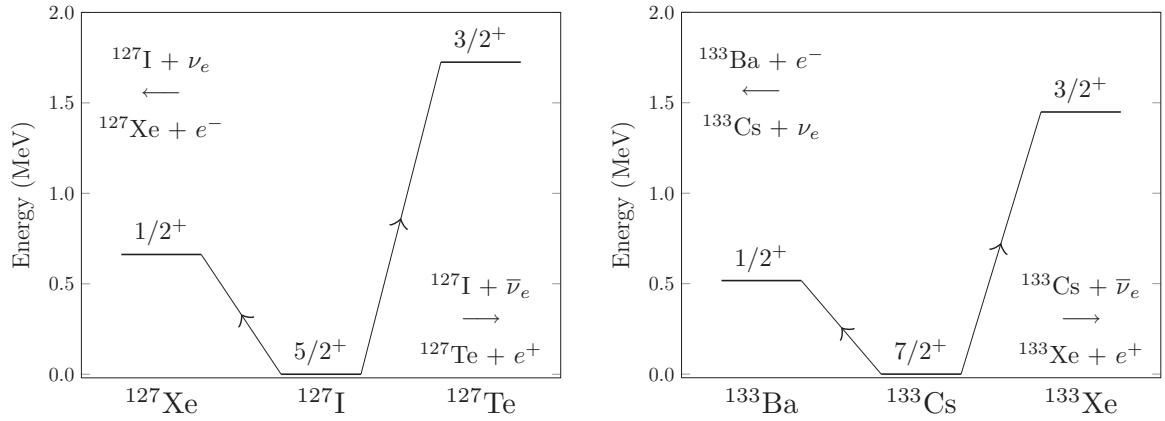

FIG. 2. The energies and spin-parities of the grounds states of the nuclei involved in the scattering reactions considered in this paper. The energies are normalized to the energy of the ground states of the initial nuclei.

the lepton (j^μ) and hadron ($\mathcal{J}^\mu$) currents with an effective Hamiltonian

$$H_{\rm eff}^{\nu/\overline{\nu}} = \frac{G}{\sqrt{2}} \int d^3\mathbf{x}\, j_\mu^{(\mp)}(\mathbf{x}) \mathcal{J}^{(\pm),\mu}(\mathbf{x}), \tag{3}$$

when the transferred four-momentum $q_\mu = k'_\mu - k_\mu = K_\mu - K'_\mu$ is small compared to the W-boson mass, i.e., $-q_\mu q^\mu \equiv Q^2 \ll M_W^2$. Here $G = G_F \cos\theta_{\rm C}$, where $G_F = 1.1664 \times 10^{-5}$ GeV is the Fermi constant and $\theta_{\rm C}$ the Cabibbo angle. We write the matrix element of the effective Hamiltonian as

$$\langle f|H_{\rm eff}^{\nu/\overline{\nu}}|i\rangle = \frac{G}{\sqrt{2}} \int d^3\mathbf{x}\, e^{-i\mathbf{q}\cdot\mathbf{x}} l_\mu^{(\mp)}(\mathbf{x}) \langle f|\, \mathcal{J}^{(\pm),\mu}(\mathbf{x})\, |i\rangle\,, \tag{4}$$

where $l_\mu^{(\mp)}(\mathbf{x}) \equiv e^{i\mathbf{q}\cdot\mathbf{x}} \langle f|\, j_\mu^{(\mp)}(\mathbf{x})\, |i\rangle$ is the lepton matrix element. The double-differential (anti)neutrino cross section off a nucleus with initial and final states $|J_{i/f}\rangle$ with energies $E_{i/f}$ can then be shown to be given by [42]

$$\left(\frac{d^2\sigma_{i\to f}}{d\Omega\, dE_{\rm exc}}\right)_{\nu/\overline{\nu}} = \frac{G^2 F(\pm Z_f, E_{k'})|\mathbf{k}'|E_{k'}}{\pi(2J_i+1)} \times \left(\sum_{J\geqslant 0} \sigma_{\rm CL}^J + \sum_{J\geqslant 1} \sigma_{\rm T}^{(\mp),J}\right), \tag{5}$$

where the Coulomb-longitudinal (CL) and transverse (T) contributions are

$$\sigma_{\rm CL}^J = (1 + a\cos\theta)|(J_f||\mathcal{M}_J(q)||J_i)|^2 + (1 + a\cos\theta - 2b\sin^2\theta)|(J_f||\mathcal{L}_J(q)||J_i)|^2 + 2\frac{E_{\rm exc}}{q}(1 + a\cos\theta + c){\rm Re}[(J_f||\mathcal{L}_J(q)||J_i)(J_f||\mathcal{M}_J(q)||J_i)^*] \tag{6}$$

and

$$\sigma_{\rm T}^{(\mp),J} = (1 - a\cos\theta + 2b\sin^2\theta)\left[|(J_f||\mathcal{T}_J^{\rm el}(q)||J_i)|^2 + |(J_f||\mathcal{T}_J^{\rm mag}(q)||J_i)|^2\right] \mp 2\frac{E_{k'} + E_k}{q}(1 - a\cos\theta - c){\rm Re}\left[(J_f||\mathcal{T}_J^{\rm mag}(q)||J_i)(J_f||\mathcal{T}_J^{\rm el}(q)||J_i)^*\right] \tag{7}$$

respectively. In the above equations, $E_{\rm exc} = E_{K'} - E_K = E_k - E_{k'}$ denotes the nuclear excitation energy,

$$q = |\mathbf{q}| = \sqrt{a^2 E_{k'}^2 + E_k^2 - 2E_k E_{k'} a\cos\theta} \tag{8}$$

the magnitude of the three-momentum transfer, and

$$a = \sqrt{1 - \frac{m_l^2}{E_{k'}^2}}, \quad b = \frac{a^2 E_k E_{k'}}{q^2}, \quad \text{and} \quad c = \frac{m_l^2}{qE_{k'}}, \tag{9}$$

where m_l is the rest mass of the final state lepton $l^\mp$.

The Coulomb interaction of the final-state lepton and daughter nucleus which distorts the wave function of the lepton is taken into account in the form of the function $F(\pm Z_f, E_{k'})$ in Eq. (5). Here, Z_f is the proton number of the daughter nucleus. For neutral current reactions we simply have $F = 1$, as the final state lepton is uncharged, but for charged-current reactions its form is more complicated. When the effective momentum $k_{\rm eff}$ and energy $E_{\rm eff}$ of the final state lepton are defined as

$$k_{\rm eff} \equiv \sqrt{E_{\rm eff}^2 - m_l^2} \quad \text{and} \quad E_{\rm eff} \equiv E_{k'} - V_{\rm C}(0), \tag{10}$$

where $V_{\rm C}(\mathbf{r})$ is the Coulomb potential due to the daughter nucleus at point $\mathbf{r}$, we can treat the effect of the distortion differently for small and large values of $k_{\rm eff}$. When $k_{\rm eff}R \ll 1$, we use a Fermi function for the function F, and for the other values of $k_{\rm eff}$ we employ the modified effective momentum approximation (MEMA) [43], where we set $F = 1$ and replace $k \equiv |\mathbf{k}'|$ and $E_{k'}$ with $k_{\rm eff}$ and $E_{\rm eff}$ respectively.

B. The nuclear current and the quenching of g_A

It is relevant for this paper to discuss the structure of the spherical tensor operators $\mathcal{M}_{JM}(q)$, $\mathcal{L}_{JM}(q)$, $\mathcal{T}^{\rm el}_{JM}(q)$, and $\mathcal{T}^{\rm mag}_{JM}(q)$ appearing in Eqs. (6) and (7) in a little more detail. The operators are defined according to [41]

$$\mathcal{M}_{JM}(q) \equiv \int d^3\mathbf{x}\, M_{JM}(q,\mathbf{x})\mathcal{J}^{(\pm)}_0(\mathbf{x}),$$
$$\mathcal{L}_{JM}(q) \equiv \frac{i}{q}\int d^3\mathbf{x}\, \nabla[M_{JM}(q,\mathbf{x})]\cdot\boldsymbol{\mathcal{J}}^{(\pm)}(\mathbf{x}),$$
$$\mathcal{T}^{\rm el}_{JM}(q) \equiv \frac{1}{q}\int d^3\mathbf{x}\big[\nabla\times\boldsymbol{M}^M_{JJ}(q,\mathbf{x})\big]\cdot\boldsymbol{\mathcal{J}}^{(\pm)}(\mathbf{x}),$$

and

$$\mathcal{T}^{\rm mag}_{JM}(q) \equiv \int d^3\mathbf{x}\,\boldsymbol{M}^M_{JJ}(q,\mathbf{x})\cdot\boldsymbol{\mathcal{J}}^{(\pm)}(\mathbf{x}), \tag{11}$$

where $\mathcal{J}^{(\pm),\mu} = (\mathcal{J}^{(\pm)}_0, -\boldsymbol{\mathcal{J}}^{(\pm)})$ and

$$M_{LM}(q,\mathbf{x}) = M_{LM}(q,r,\theta,\phi) \equiv j_L(qr)Y^L_M(\theta,\phi)$$
$$\text{and } \boldsymbol{M}^M_{JL}(q,\mathbf{x}) = \boldsymbol{M}^M_{JL}(q,r,\theta,\phi) \equiv j_L(qr)\boldsymbol{\mathcal{Y}}^M_{JL1}(\theta,\phi), \tag{12}$$

with j_L being the spherical Bessel function of order L and $(\boldsymbol{\mathcal{Y}}^M_{JL1})Y^L_M$ the (vector-)spherical harmonic function. The nuclear current operator contains both vector and axial-vector parts $\mathcal{J}^{(\pm),\mu} = J^{(\pm),\mu}_{\rm V} - J^{(\pm),\mu}_{\rm A}$ and as a result so do the spherical tensor operators above. They can therefore be separated into vector and axial-vector parts [e.g., $\mathcal{M}_{JM}(q) = M^{\rm V}_{JM}(q) - M^{\rm A}_{JM}(q)$] and we can consider their matrix elements separately.

The first and second quantized vector/axial-vector nuclear current operators are written in terms of the free particle (box-normalized plane wave) states $|\mathbf{p}\sigma\rangle$, $\langle\mathbf{x}|\mathbf{p},\sigma\rangle = \phi_{\mathbf{p},\sigma}(\mathbf{x})$ of momentum $\mathbf{p}$ and spin σ as [41,44]

$$J^{(\pm),\mu}_{\rm V/A}(\mathbf{x}) = \sum_{i=1}^{\substack{N\\Z}} J^{(\pm),\mu}_{{\rm V/A},i}\,\delta^{(3)}(\mathbf{x}-\mathbf{x}_i) \tag{13}$$

and

$$J^{(\pm),\mu}_{\rm V/A}(\mathbf{x}) = \sum_{\mathbf{p}',\sigma',\mathbf{p},\sigma} {}^{\rm p}_{\rm n}\langle\mathbf{p}',\sigma'|J^{(\pm),\mu}_{\rm V/A}|\mathbf{p},\sigma\rangle^{\rm n}_{\rm p}\, c^\dagger_{{\rm p}_{\rm n}\mathbf{p}'\sigma'}c_{{\rm p}_{\rm n}\mathbf{p}\sigma} \tag{14}$$

respectively, with

$${}^{\rm p}_{\rm n}\langle\mathbf{p}',\sigma'|J^{(\pm),\mu}_{\rm V/A}(\mathbf{x})|\mathbf{p},\sigma\rangle^{\rm n}_{\rm p} = \int d^3\mathbf{y}\,\phi^\dagger_{{\rm p}_{\rm n}\mathbf{p}'\sigma'}(\mathbf{y})J^{(\pm),\mu}_{{\rm V/A},1}(\mathbf{y}) \times\delta^{(3)}(\mathbf{x}-\mathbf{y})\phi_{{\rm p}_{\rm n}\mathbf{p}\sigma}(\mathbf{y}), \tag{15}$$

where $J^{(\pm),\mu}_{{\rm V/A},i(1)}$ is the current due to the ith (a single) nucleon and $c^\dagger_{{\rm p}_{\rm n}\mathbf{p}\sigma}$ and $c_{{\rm p}_{\rm n}\mathbf{p}\sigma}$ are the creation and annihilation operators of the plane wave states for $^{\rm protons}_{\rm neutrons}$. The most general forms of the matrix elements $\langle\mathbf{p}',\sigma'|\,J^{(\pm),\mu}_{\rm V/A}\,|\mathbf{p},\sigma\rangle$ that satisfy Lorentz covariance, parity conservation, time-reversal invariance, and isospin invariance can be written by using the Dirac equation at the origin as (assuming no second-class currents) [45]

$${}^{\rm p}_{\rm n}\langle\mathbf{p}',\sigma'|J^{(\pm),\mu}_{\rm V}(0)|\mathbf{p},\sigma\rangle^{\rm n}_{\rm p} = \frac{1}{V}\overline{u}^{\rm p}_{\rm n}(\mathbf{p}',\sigma') \times\left[F^{\rm CC}_1(q^2)\gamma^\mu - \frac{i}{2m_{\rm N}}F^{\rm CC}_2(q^2)\sigma^{\mu\nu}q_\nu\right]u^{\rm p}_{\rm n}(\mathbf{p},\sigma) \tag{16}$$

and

$${}^{\rm p}_{\rm n}\langle\mathbf{p}',\sigma'|J^{(\pm),\mu}_{\rm A}(0)|\mathbf{p},\sigma\rangle^{\rm n}_{\rm p} = \frac{1}{V}\overline{u}^{\rm p}_{\rm n}(\mathbf{p}',\sigma')\big[F^{\rm CC}_{\rm A}(q^2)\gamma_5\gamma^\mu + F^{\rm CC}_{\rm P}(q^2)\gamma_5 q^\mu\big]u^{\rm p}_{\rm n}(\mathbf{p},\sigma), \tag{17}$$

where V is the quantization volume of the plane waves, $m_{\rm N}$ the nucleon mass, and $[\overline{u}^{\rm p}_{\rm n}(\mathbf{p},\sigma)]$ $u^{\rm p}_{\rm n}(\mathbf{p},\sigma)$ the [adjoint] Dirac spinor of a $^{\rm proton}_{\rm neutron}$. The form factors $F^{\rm CC}_1$, $F^{\rm CC}_2$, $F^{\rm CC}_{\rm A}$, and $F^{\rm CC}_{\rm P}$ are used to take into account the finite size of the nucleons. The right-hand sides of the above equations can then be expanded in powers of $m_{\rm N}^{-1}$ up to second order and compared to the matrix element of the second-quantized operator of Eq. (14) at the origin to obtain the form of the operators $J^{(\pm),\mu}_{\rm V/A,1}$. Then an expression for the cross section in terms of the form factors can eventually be obtained [41].

For the purposes of the present paper, the axial-vector form factor $F^{\rm CC}_{\rm A}(q^2)$ can be modeled using the dipole form

$$F^{\rm CC}_{\rm A}(q^2) = \frac{F^{\rm CC}_{\rm A}(0)}{\left(1+\frac{q^2}{M^2_{\rm A}}\right)^2}, \tag{18}$$

where $M_{\rm A} = 1.014$ GeV and $F^{\rm CC}_{\rm A}(0) = g_{\rm A}$ is the weak axial-vector coupling constant. The bare value of $g_{\rm A}$ is predicted by the partially conserved axial-vector current (PCAC) hypothesis [46], and can be measured from some weak process, such as the decay of a free neutron into a proton. The currently accepted value of this is $g_{\rm A} = -1.27641(45)_{\rm stat}(33)_{\rm sys}$ [47]. However, the effective value of $g_{\rm A}$ in nuclear medium typically needs to be quenched with respect to the bare value in order to obtain acceptable agreement with experimental results [34,35,48,49]. This is mainly due to the limitations in the single-nucleon valence and many-nucleon configuration spaces, and the neglect of three-nucleon forces in numerical calculations. Further quenching arises from nuclear-medium effects, such as the meson-exchange many-body currents that are not included in the one-nucleon impulse approximation, and non-nucleonic degrees of freedom (e.g., Δ baryons) that are usually neglected [36].

In the (anti)neutrino-nucleus scattering calculations, typically an unquenched or moderately quenched, $g_{\rm A,eff} = -1.0$, value has been used [39]. In the context of these scatterings, little has been done in exploring systematically the degree of quenching of the axial coupling. Contrary to this, for some other neutrino-related processes, like beta decays and double beta decays, a lot of systematic investigations have been performed in order to pin down the degree of $g_{\rm A}$ quenching in these processes [36,39,50,51]. One of these systematic studies is conducted in the nuclear mass region $A = 100$–136 [52], relevant for the present work in terms of the nuclear mass range and the assumed nuclear many-body

frameworks, namely the quasiparticle random-phase approximation (QRPA) and proton-neutron QRPA (pnQRPA). The analyses of Ref. [52], performed for Gamow-Teller beta and two-neutrino double beta decays, revealed an average piecewise linear dependence of $g_{\rm A,eff}$ on the mass number, $g_{\rm A,eff} = (A-86)/60$, within the mass range $A = 122$–136. This linear fit would suggest values $g_{\rm A,eff} \approx -0.683$ for ^{127}I and $g_{\rm A,eff} \approx -0.783$ for ^{133}Cs. Also some IBM-2 (microscopic interacting boson model) and ISM (interacting shell model) based studies in this region implied similarly quenched $g_{\rm A,eff}$ values [36].

Here one has to note that the momentum transfers in the neutrino-nucleus scattering, discussed in the present work, are much larger than in the Gamow-Teller type of beta and two-neutrino double beta decays mentioned above. This means that in addition to the allowed Gamow-Teller type of contributions, corresponding to the s partial wave of the involved leptons, a non-negligible contribution arises from the so-called forbidden transitions corresponding to higher partial waves of the involved leptons. At zero momentum transfer these forbidden transitions can be studied using forbidden beta decays. These studies [53,54] suggest that $g_{\rm A,eff}$ would be even more radically quenched for the forbidden decays than for the allowed ones. The study of first-forbidden unique beta decays in the mass range $A = 72$–136, performed in [53], suggests a value $g^{\rm forb}_{\rm A,eff} = 0.57$, when the pnQRPA-computed beta-decay rates are compared with the measured ones. Even stronger quenchings are suggested for the higher-forbidden beta decays in [54]; see the discussion in [36].

Based on the above discussion, we can build a (conservative) quenching model for $g_{\rm A}$ such that for both the allowed Gamow-Teller and the forbidden transitions we use the results of the linear fit. We can test this quenching model against experimental data for the scattering of the stopped-pion neutrinos off ^{127}I, as discussed in Sec. III B.

C. Nuclear structure

The initial- and final-state nuclear wave functions used in our calculations were modeled by using the same formalism as in our previous work concerning the neutral-current (anti)neutrino-nucleus scattering off ^{127}I and ^{133}Cs, namely the MQPM [55,56]. For a brief recap, the MQPM is a quasiparticle based nuclear model which is built upon the quasiparticle random-phase approximation (QRPA), which in turn is based on the BCS model of the atomic nucleus. The BCS-quasiparticle creation and annihilation operators $a^\dagger_\alpha$ and $\tilde{a}_\alpha$ [using the standard Baranger notation $\alpha \equiv (a, m_\alpha) \equiv (n_a, l_a, j_a, m_\alpha)$ for the quantum numbers] are obtained from particle-hole creation and annihilation operators $c^\dagger_\alpha$ and $\tilde{c}_\alpha$ by the Bogolyubov-Valatin transform,

$$a^\dagger_\alpha = u_a c_\alpha + v_a \tilde{c}_\alpha, \quad \tilde{a}_\alpha = u_a \tilde{c}_\alpha - v_a c^\dagger_\alpha, \tag{19}$$

where u_a and v_a are the occupation and vacancy amplitudes respectively.

After solving the BCS occupation amplitudes, the quasiparticle operators can be coupled together to form the QRPA phonon operators [49]

$$Q^\dagger_{J_\omega,\pi_\omega,k_\omega} \equiv Q^\dagger_\omega = \sum_{a\leqslant b} \left[X^\omega_{ab} A^\dagger(JM) - Y^\omega_{ab} \tilde{A}(JM)\right], \tag{20}$$

where

$$A^\dagger_{ab}(JM) \equiv \frac{\sqrt{1+\delta_{ab}(-1)^J}}{1+\delta_{ab}} [a^\dagger_a a^\dagger_b]_{JM},$$
$$\tilde{A}_{ab}(JM) = (-1)^{J+M} A_{ab}(J-M). \tag{21}$$

The quantum numbers $(J_\omega, \pi_\omega, k_\omega)$ of a phonon denote its angular momentum, parity, and enumeration number respectively. The phonon operators can then, in turn, be used to construct the MQPM excitation creation operators

$$\Gamma^\dagger_i(JM) = \sum_n C^i_n a^\dagger_{nJM} + \sum_{a\omega} D^i_{a\omega} [a^\dagger_a Q^\dagger_\omega]_{JM}. \tag{22}$$

The amplitudes X^ω and Y^ω can be solved from the QRPA equations

$$\begin{pmatrix} \mathsf{A} & \mathsf{B} \\ -\mathsf{B}^* & -\mathsf{A}^* \end{pmatrix} \begin{pmatrix} \mathsf{X}^\omega \\ \mathsf{Y}^\omega \end{pmatrix} = E_\omega \begin{pmatrix} \mathsf{X}^\omega \\ \mathsf{Y}^\omega \end{pmatrix}, \tag{23}$$

after which the amplitudes C^i and D^i can be solved from the MQPM equations

$$\begin{pmatrix} A & B \\ B^{\rm T} & A' \end{pmatrix} \begin{pmatrix} C^i \\ D^i \end{pmatrix} = \Omega_i \begin{pmatrix} 1 & 0 \\ 0 & N \end{pmatrix} \begin{pmatrix} C^i \\ D^i \end{pmatrix}. \tag{24}$$

The details of solving these equations along with the nature of the submatrices A, B, A, A', B, and N are discussed in [49].

The nuclear models discussed thus far were applied in the same manner as in our previous paper, and the details of this procedure are discussed there. We will give a brief recap of this here. In the BCS-calculations for the even-even reference nuclei, the lowest theoretical quasiparticle energies were fitted to the experimental proton and neutron pairing gaps defined by the equations

$$\Delta_\pi(A,Z) = \tfrac{1}{4}(-1)^{Z+1}[S_{\rm p}(A+1,Z+1) - 2S_{\rm p}(A,Z) + S_{\rm p}(A-1,Z-1)] \tag{25}$$

and

$$\Delta_\nu(A,Z) = \tfrac{1}{4}(-1)^{N+1}[S_{\rm n}(A+1,Z) - 2S_{\rm n}(A,Z) + S_{\rm n}(A-1,Z)], \tag{26}$$

given in terms of the experimental proton and neutron separation energies $S_{\rm p}$ and $S_{\rm n}$. The single-particle energies used in the calculations were obtained from the Coulomb corrected Woods-Saxon potential using the Bohr-Mottelson parametrization [57] with adjustments to the energies of the states near the Fermi surface. These adjustments were made to improve agreement with the theoretical and experimental spectra, and they are listed in Table I. The QRPA calculations for the even-even reference nuclei were performed by fitting the energies of the lowest theoretical states of natural parity up to and including 6^+ to their experimental counterparts, by scaling the two-body matrix elements of said multipolarities in the matrices A and B with the phenomenological particle-particle and particle-hole strength parameters $g_{\rm pp}$ and $g_{\rm ph}$

TABLE I. Adjustments to the energies of the single-particle Woods-Saxon orbitals (in MeV) for all MQPM reference nuclei.

Orbital	^{126}Te	^{128}Xe	^{132}Xe	^{134}Ba
$1d_{5/2,\pi}$	–	–	–	+0.03
$0g_{7/2,\pi}$	−0.15	−0.20	−0.35	−0.70
$0h_{11/2,\pi}$	−0.60	−0.30	−0.60	−0.50
$2s_{1/2,\pi}$	–	–	–	–
$1d_{3/2,\pi}$	–	–	–	–
$1d_{5/2,\nu}$	–	–	–	–
$0g_{7/2,\nu}$	+1.00	+2.00	–	–
$2s_{1/2,\nu}$	+0.90	+0.60	+0.30	+1.00
$1d_{3/2,\nu}$	+0.60	−0.30	+0.50	+0.14
$0h_{11/2,\nu}$	−1.00	−1.13	−1.00	−1.00

[58,59]. The results of the QRPA calculations were then used to perform the MQPM calculations for the odd-A nuclei of interest. The resulting theoretical spectra along with the corresponding experimental spectra for the neutron-odd nuclei are illustrated in Figs. 3 [60] and 4 [61]. The corresponding graphs for the proton-odd nuclei and the QPRA results for the even-even reference nuclei are found in our previous paper [62]. The same values as in the QRPA calculations for the parameters g_{pp} and g_{ph} were also used in the MQPM calculations, and all fitting to experimental data was done at the BCS and QRPA level of calculations.

It should be noted that the nuclear-structure calculations for the nuclei considered in our previous work, namely ^{127}I and ^{133}Cs and their corresponding even-even reference nuclei ^{126}Te, ^{128}Xe, ^{132}Xe, and ^{134}Ba, were identical to the calculations needed for this paper, and the previously obtained results were naturally used for them. The charged-current scattering final state nuclei ^{127}Xe, ^{127}Te, ^{133}Ba, and ^{133}Xe can be modeled using the same even-even reference nuclei as the initial nuclei [e.g., the QRPA results for ^{134}Ba can be used to model ^{133}Cs (^{133}Ba) by performing a proton(neutron)-odd MQPM calculation]. This was in fact already taken into account in our previous work by adjusting the neutron single-particle energies near the Fermi surface to improve the agreement between the theoretical and experimental spectra of the neutron-odd

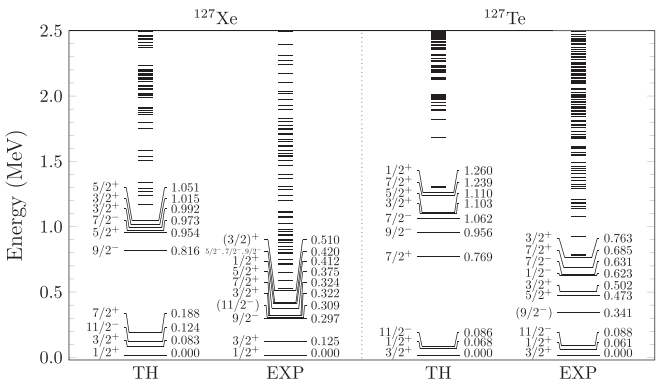

FIG. 3. Experimental and MQPM-computed energy spectra of ^{127}Xe and ^{127}Te from the reference nuclei ^{128}Xe and ^{126}Te, respectively.

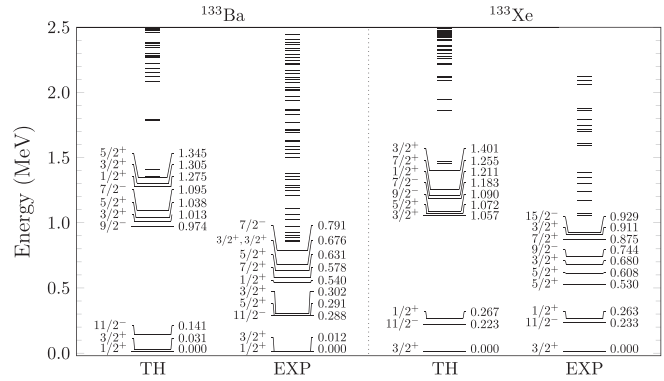

FIG. 4. Experimental and MQPM-computed energy spectra of ^{133}Ba and ^{133}Xe from the reference nuclei ^{134}Ba and ^{132}Xe, respectively.

charged-current scattering final nuclei, despite the fact that the neutron-odd nuclei were not considered in the mentioned work. The reason for this was to make the neutral-current and charged-current scattering results as comparable to each other as possible by using the same even-even reference nuclei in both calculations.

III. RESULTS

A. Scattering cross sections

The results for the total neutrino scattering cross sections as functions of the energy of the incoming neutrino for the reactions of Eq. (2) are presented in Table II. Here we have used the conservative estimate for the quenching of g_A, namely quenching the axial coupling in the same way for the allowed and forbidden transitions. We also give the decomposition of the total cross sections to the vector, axial-vector, and interference parts. The cross sections were obtained by first computing the double-differential cross section of Eq. (5), numerically integrating over the scattering angle and summing over the contributions from individual final states. These cross sections are also illustrated in Fig. 5. It can be clearly seen that the neutrino scattering cross sections are noticeably larger than the corresponding cross sections for antineutrino scattering for both nuclei. This result was expected based on the differences in the threshold energies between the different reactions, as discussed at the start of the previous section. This difference in cross sections is more pronounced at lower incoming (anti)neutrino energies and diminishes steadily as the energy of the lepton increases, as the differences between threshold energies are independent of the projectile energy. The differences between the two nuclei for the same types of reactions are relatively small. For neutrino scattering, the cross sections are slightly higher for the $\nu_e + {}^{133}\mathrm{Cs} \longrightarrow e^- + {}^{133}\mathrm{Ba}$ reaction compared to the $\nu_e + {}^{127}\mathrm{I} \longrightarrow e^- + {}^{127}\mathrm{Xe}$ reaction, but for the lowest of incoming neutrino energies where the differences in contributions from individual final nuclear states between the two odd-A nuclei can be significant. The cause of this is mainly due to the higher $g_{A,\mathrm{eff}}$ parameter value used for the former. Similar behavior is also observed for the antineutrino scattering, although in this case the cross

TABLE II. Total neutrino (ν) and antineutrino ($\bar{\nu}$) scattering cross sections ($\sigma_{\text{Tot.}}$), computed using our quenching model for $g_{\text{A,eff}}$ (see Sec. II B), as functions of the energy of the incoming lepton for both nuclei of interest. The decompositions of the total cross sections into the vector (σ_{V}), axial-vector (σ_{A}) and interference (σ_{I}) contributions are also provided. Here it should be noted that one can obtain the total scattering cross sections for any value of g_{A} by multiplying the axial contributions by the ratio $g_{\text{A}}^2/g_{\text{A,eff}}^2$ and the interference contributions by the ratio $g_{\text{A}}/g_{\text{A,eff}}$. The format in which the data is presented is $R(e)$, and the cross sections are obtained by $\sigma(E_{\mathbf{k}}) = R \times 10^e \times D$. The units D are $(10^{-46})10^{-42}$ cm^2 for (anti)neutrino scattering.

	Initial nucleus															
	^{127}I								^{133}Cs							
	Final nucleus								Final nucleus							
	^{127}Xe (ν)				^{127}Te ($\bar{\nu}$)				^{133}Ba (ν)				^{133}Xe ($\bar{\nu}$)			
$E_{\mathbf{k}}$ (MeV)	$\sigma_{\text{Tot.}}$	σ_{V}	σ_{A}	σ_{I}	$\sigma_{\text{Tot.}}$	σ_{V}	σ_{A}	σ_{I}	$\sigma_{\text{Tot.}}$	σ_{V}	σ_{A}	σ_{I}	$\sigma_{\text{Tot.}}$	σ_{V}	σ_{A}	σ_{I}
5.0	2.584(0)	5.289(−1)	2.000(0)	5.603(−2)	9.863(1)	3.087(−1)	1.016(2)	−3.240(0)	2.360(0)	1.237(−1)	2.173(0)	6.336(−2)	5.779(0)	4.372(−1)	5.415(0)	−7.292(-2)
10.0	5.999(1)	2.366(1)	3.360(1)	2.723(0)	1.533(3)	2.072(2)	1.402(3)	−7.655(1)	6.814(1)	1.972(1)	4.509(1)	3.328(0)	8.634(2)	1.132(2)	7.906(2)	−4.034(1)
15.0	2.195(2)	8.952(1)	1.158(2)	1.417(1)	7.750(3)	1.620(3)	6.684(3)	−5.535(2)	2.583(2)	8.593(1)	1.552(2)	1.720(1)	4.710(3)	1.117(3)	4.054(3)	−4.617(2)
20.0	4.610(2)	1.900(2)	2.298(2)	4.114(1)	2.126(4)	5.497(3)	1.833(4)	−2.573(3)	5.428(2)	1.910(2)	3.009(2)	5.086(1)	1.469(4)	4.149(3)	1.283(4)	−2.289(3)
25.0	7.020(2)	2.938(2)	3.261(2)	8.210(1)	4.508(4)	1.372(4)	3.924(4)	−7.877(3)	8.089(2)	2.990(2)	4.151(2)	9.483(1)	3.454(4)	1.083(4)	3.079(4)	−7.077(3)
30.0	9.185(2)	3.847(2)	4.146(2)	1.191(2)	8.256(4)	2.864(4)	7.275(4)	−1.884(4)	1.047(3)	3.915(2)	5.234(2)	1.325(2)	6.824(4)	2.318(4)	6.204(4)	−1.697(4)
35.0	1.175(3)	4.821(2)	5.241(2)	1.692(2)	1.365(5)	5.276(4)	1.218(5)	−3.801(4)	1.333(3)	4.901(2)	6.566(2)	1.858(2)	1.190(5)	4.339(4)	1.102(5)	−3.452(4)
40.0	1.473(3)	5.928(2)	6.419(2)	2.384(2)	2.106(5)	8.858(4)	1.906(5)	−6.855(4)	1.652(3)	5.965(2)	7.969(2)	2.583(2)	1.902(5)	7.367(4)	1.788(5)	−6.232(4)
45.0	1.794(3)	7.151(2)	7.596(2)	3.191(2)	3.107(5)	1.384(5)	2.835(5)	−1.112(5)	1.986(3)	7.129(2)	9.317(2)	3.417(2)	2.861(5)	1.160(5)	2.716(5)	−1.015(5)
50.0	2.125(3)	8.427(2)	8.763(2)	4.064(2)	4.464(5)	2.076(5)	4.131(5)	−1.743(5)	2.328(3)	8.349(2)	1.066(3)	4.278(2)	4.183(5)	1.751(5)	4.018(5)	−1.587(5)
55.0	2.480(3)	9.803(2)	9.981(2)	5.018(2)	6.347(5)	3.122(5)	5.928(5)	−2.704(5)	2.689(3)	9.643(2)	1.202(3)	5.232(2)	6.071(5)	2.670(5)	5.902(5)	−2.501(5)
60.0	2.846(3)	1.121(3)	1.116(3)	6.091(2)	8.883(5)	4.645(5)	8.308(5)	−4.070(5)	3.054(3)	1.096(3)	1.332(3)	6.266(2)	8.662(5)	4.004(5)	8.340(5)	−3.742(5)
65.0	3.216(3)	1.269(3)	1.228(3)	7.192(2)	1.203(6)	6.656(5)	1.137(6)	−6.000(5)	3.413(3)	1.228(3)	1.454(3)	7.309(2)	1.192(6)	5.767(5)	1.167(6)	−5.514(5)
70.0	3.582(3)	1.417(3)	1.336(3)	8.290(2)	1.581(6)	9.329(5)	1.506(6)	−8.573(5)	3.763(3)	1.359(3)	1.569(3)	8.348(2)	1.588(6)	8.163(5)	1.567(6)	−7.960(5)
75.0	3.947(3)	1.564(3)	1.440(3)	9.417(2)	2.015(6)	1.266(6)	1.925(6)	−1.176(6)	4.108(3)	1.489(3)	1.680(3)	9.396(2)	2.037(6)	1.113(6)	2.019(6)	−1.095(6)
80.0	4.307(3)	1.715(3)	1.538(3)	1.054(3)	2.485(6)	1.655(6)	2.373(6)	−1.544(6)	4.447(3)	1.619(3)	1.783(3)	1.045(3)	2.520(6)	1.459(6)	2.499(6)	−1.437(6)
85.0	4.663(3)	1.867(3)	1.628(3)	1.168(3)	2.983(6)	2.103(6)	2.843(6)	−1.963(6)	4.781(3)	1.751(3)	1.879(3)	1.151(3)	3.028(6)	1.854(6)	2.994(6)	−1.820(6)
90.0	5.008(3)	2.019(3)	1.712(3)	1.276(3)	3.504(6)	2.600(6)	3.315(6)	−2.411(6)	5.102(3)	1.881(3)	1.969(3)	1.252(3)	3.548(6)	2.288(6)	3.489(6)	−2.229(6)
95.0	5.340(3)	2.169(3)	1.790(3)	1.380(3)	4.039(6)	3.140(6)	3.787(6)	−2.888(6)	5.413(3)	2.009(3)	2.054(3)	1.350(3)	4.076(6)	2.755(6)	3.974(6)	−2.654(6)
100.0	5.664(3)	2.317(3)	1.865(3)	1.482(3)	4.584(6)	3.713(6)	4.247(6)	−3.376(6)	5.718(3)	2.136(3)	2.135(3)	1.446(3)	4.604(6)	3.247(6)	4.446(6)	−3.090(6)

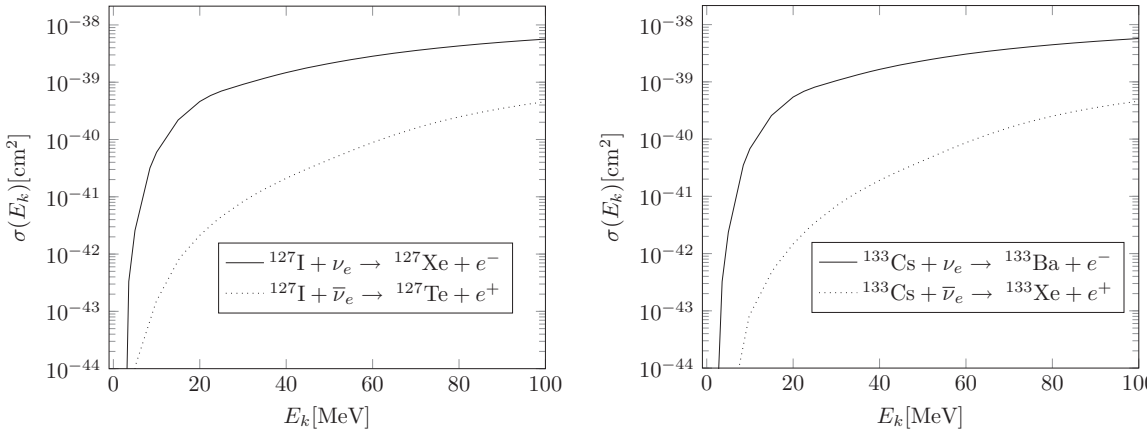

FIG. 5. Total cross section as function of the incoming (anti)neutrino energy for all the scattering reactions of interest.

section of the $\overline{\nu}_e + {}^{127}\mathrm{I} \longrightarrow e^+ + {}^{127}\mathrm{Te}$ reaction remains larger than that of the $\overline{\nu}_e + {}^{133}\mathrm{Cs} \longrightarrow e^+ + {}^{133}\mathrm{Xe}$ reaction until relatively high ($\gtrapprox 70$ MeV) antineutrino energies.

B. Flux-averaged stopped-pion neutrino cross sections

We also report results for (anti)neutrino-flux-averaged cross sections involving two neutrino sources: Accelerator based stopped-pion decay and astrophysical supernova (anti)neutrinos. Stopped-pion neutrinos are produced in the decay chain of π^+ in the reactions

$$\pi^+ \longrightarrow \mu^+ + \nu_\mu \quad \text{and} \quad \mu^+ \longrightarrow e^+ + \nu_e + \overline{\nu}_\mu. \tag{27}$$

The first reactions is a two-body decay and the produced ν_μ are thus monochromatic in energy as a result. We used the value $E_{\nu_\mu} = 29.8$ MeV in our calculations. The spectra of the electron neutrinos and muon antineutrinos produced in the second reaction are continuous, and for the former we utilized the commonly used model

$$p(E_{\nu_e}) = 96\frac{E_{\nu_e}^2}{m_\mu^4}(m_\mu - 2E_{\nu_e}), \tag{28}$$

where m_μ is the muon mass and $E_{\nu_e} \in [0, m_\mu/2]$.

The flux-averaged cross sections $\langle\sigma\rangle$ were computed by folding the energy dependent cross sections with the above (anti)neutrino energy distributions, i.e.,

$$\langle\sigma\rangle = \int_0^\infty dE_\nu \sigma(E_\nu) p(E_\nu). \tag{29}$$

The results are presented in Table III. Of particular interest is the cross section for stopped-pion electron neutrino scattering off ^{127}I, as this cross section was recently experimentally measured by the COHERENT Collaboration. Their reported cross sections were $(9.2^{+2.1}_{-1.8}) \times 10^{-40}$ cm^2 for the inclusive reaction $\nu_e + {}^{127}\mathrm{I} \longrightarrow e^- + {}^{127}\mathrm{Xe}^*$ and $(5.2^{+3.4}_{-3.1}) \times 10^{-40}$ cm^2 for the exclusive reaction $\nu_e + {}^{127}\mathrm{I} \longrightarrow e^- + {}^{127}\mathrm{Xe}^*$(bound states) [14]. Our corresponding result for the inclusive reaction was computed to be 10.6×10^{-40} cm^2, which was obtained by using our quenching model. This in good agreement with the reported experimental result. An earlier theoretical study [25] utilizing the local density approximation, taking into account Pauli blocking, Fermi motion effects and renormalization of weak transition strengths in the nuclear medium, found a result of 12.53×10^{-40} cm^2 for the inclusive cross section,

TABLE III. Total folded neutrino (ν) and antineutrino ($\bar{\nu}$) scattering cross sections, computed using our quenching model for $g_{\mathrm{A,eff}}$ (see Sec. II B), for both nuclei of interest. Also included are the individual contributions to the total folded cross sections, namely the CL and T contributions of Eqs. (6) and (7), along with the vector (V), axial-vector (A), and interference (I) contributions. Here it should be noted that one can obtain the total folded scattering cross sections for any value of g_{A} by multiplying the axial contributions by the ratio $g_{\mathrm{A}}^2/g_{\mathrm{A,eff}}^2$ and the interference contributions by the ratio $g_{\mathrm{A}}/g_{\mathrm{A,eff}}$. The results are for supernova neutrino spectra with the choices $\alpha = 0$ and $\alpha = 3$ for the degeneracy parameter, and stopped-pion (π) electron neutrino spectrum. The format in which the data is presented is the same as in Table II and the units are 10^{-43} cm^2.

	Initial nucleus			
	^{127}I		^{133}Cs	
	Final nucleus		Final nucleus	
	^{127}Xe (ν_e)	^{127}Te ($\overline{\nu}_e$)	^{133}Ba (ν_e)	^{133}Xe ($\overline{\nu}_e$)
$\mathrm{CL}_{\alpha=0}$	6.894(2)	4.569(0)	6.917(2)	3.515(0)
$\mathrm{CL}_{\alpha=3}$	6.232(2)	3.193(0)	6.201(2)	2.354(0)
CL_{π}	4.225(3)	–	4.360(3)	–
$\mathrm{T}_{\alpha=0}$	9.037(2)	1.018(1)	1.157(3)	7.901(0)
$\mathrm{T}_{\alpha=3}$	8.054(2)	7.996(0)	1.042(3)	5.755(0)
T_{π}	6.360(3)	–	7.569(3)	–
$\mathrm{V}_{\alpha=0}$	6.509(2)	4.709(0)	6.329(2)	3.737(0)
$\mathrm{V}_{\alpha=3}$	5.818(2)	3.157(0)	5.576(2)	2.433(0)
V_{π}	4.305(3)	–	4.332(3)	–
$\mathrm{A}_{\alpha=0}$	8.030(2)	1.300(1)	1.051(3)	1.034(1)
$\mathrm{A}_{\alpha=3}$	7.360(2)	9.782(0)	9.722(2)	7.228(0)
A_{π}	4.681(3)	–	5.846(3)	–
$\mathrm{I}_{\alpha=0}$	1.391(2)	−2.960(0)	1.650(2)	−2.657(0)
$\mathrm{I}_{\alpha=3}$	1.108(2)	−1.749(0)	1.324(2)	−1.553(0)
I_{π}	1.601(3)	–	1.751(3)	–
$\mathrm{Tot.}_{\alpha=0}$	1.593(3)	1.475(1)	1.849(3)	1.142(1)
$\mathrm{Tot.}_{\alpha=3}$	1.429(3)	1.119(1)	1.662(3)	8.108(0)
$\mathrm{Tot.}_{\pi}$	1.059(4)	–	1.193(4)	–

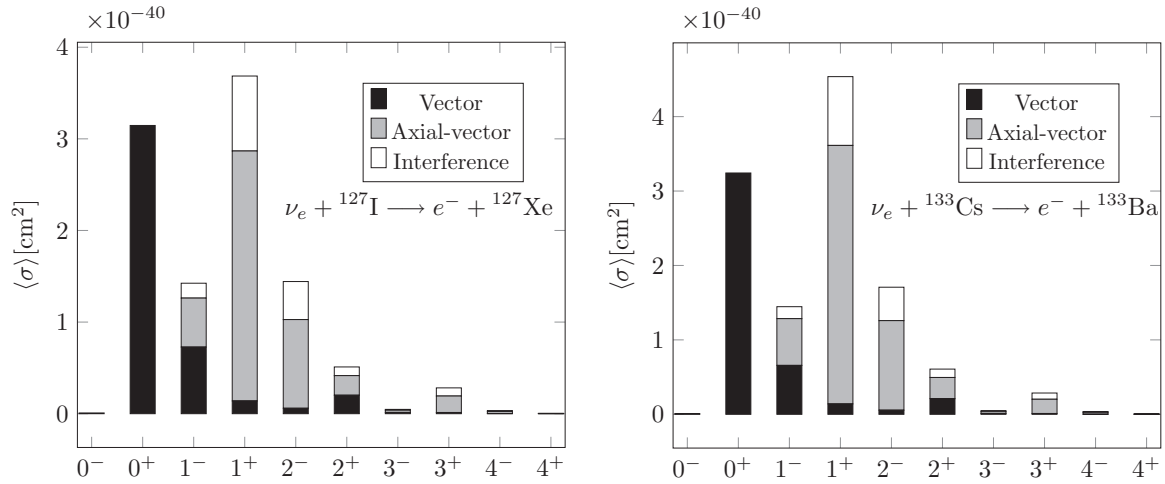

FIG. 6. Contributions of different multipoles to the total folded stopped-pion neutrino cross section for scattering off ^{127}I (left) and ^{133}Cs (right). The parts with different tensorial character (vector, axial-vector, interference) for each individual multipole contribution are also visualized. Higher multipoles not present in the graphs have vanishingly small contributions.

which is also in relatively good agreement with both our result and experiment.

To obtain an accurate theoretical result for the cross section of the exclusive channel would require calculation of the neutron emission probabilities of different final nuclear states of ^{127}Xe that are above the neutron separation energy of 7.246 MeV, which is outside the scope of this work. We can, however, compute a lower bound for the exclusive channel by summing up the contribution from all the final states below the neutron emission threshold. The lower bound obtained in this manner was 6.1×10^{-40} cm^2, which is compatible with the experimental result. Regarding this, it should be noted that the uncertainties in the experimental exclusive result are rather large, and thus no definite conclusions can be drawn from this comparison. Nevertheless, an earlier result of $[2.84 \pm 0.91(\text{stat}) \pm 0.25(\text{syst})] \times 10^{-40}$ cm^2 for the exclusive cross section obtained at the Los Alamos Meson Physics Facility (LAMPF) exists [26], which is in agreement with the most recent COHERENT result (due to large uncertainties in the latter), and in disagreement with our theoretical estimate for the lower bound.

The contributions from different multipoles to the total folded cross section of stopped-pion electron neutrinos off ^{127}I, along with the scattering off ^{133}Cs are presented in Fig. 6. In the figure it can clearly be seen that the allowed 0^+ and 1^+ multipoles are the most prominent, while the forbidden transitions still contribute significantly. All the axial-vector contributions together are responsible for ∼44% of the total folded cross section for the scattering off ^{127}I, and a total of ∼58% of the axial-vector contributions are from the allowed 1^+ multipole. At this moment no data are available for the scattering cross section off ^{133}Cs meaning that the results obtained for this nucleus currently serve as predictions for future experiments. The differences between the multipole profiles between the two nuclei are also minute aside from the absolute values of the contributions, which are larger for ^{133}Cs as were the total folded cross sections. The relative proportions of the contributions (e.g., allowed to forbidden) can be seen to be highly similar on the other hand.

Thus far in our calculations we have used the (conservative) quenching model of $g_{\text{A,eff}} \approx -0.683$ for all multipole transitions in ^{127}I. A more "radical" quenching scheme would be to adopt the value $g_{\text{A,eff}}^{\text{forb}} = 0.57$ for all forbidden transitions, as suggested by the study [53]. Some 42% of the axial contribution in Fig. 6 comes from the forbidden transitions. Applying the quenching $g_{\text{A,eff}}^{\text{forb}} = 0.57$ on this part of the axial contribution would bring our conservative estimates for the stopped-pion inclusive cross sections, 10.6×10^{-40} cm^2 for ^{127}I and 11.9×10^{-40} cm^2 for ^{133}Cs, to values 9.9×10^{-40} cm^2 for ^{127}I and 10.6×10^{-40} cm^2 for ^{133}Cs. Hence, the additional quenching coming from the forbidden transitions does not affect much the final values of cross sections. Anyway, nothing definitive can be stated about the superiority of either quenching scheme since in the case of ^{127}I both are in agreement with the experimental result owing to its large error bars.

In addition to the multipole profiles, other data of interest include the contributions to the total folded cross sections from individual final nuclear states. These are presented for the conservative quenching estimate in Fig. 7. For charged-current scattering most of the contributions for both nuclei come from a high number of individual states spread over a relatively wide range in energy. It is worth mentioning that, in comparison, we found in our previous paper in the context of supernova neutrino scattering that the neutral-current contributions came from a relatively small number of highly contributing states, located particularly in the ∼8–10 MeV range, corresponding likely to spin-flip $M1$ giant resonances [62].

Another difference compared to the earlier neutral-current results is that while they and the new charged-current results do share the feature that the most highly contributing states are composed of mainly states that can be reached from the ground state of the mother nucleus via an allowed transition,

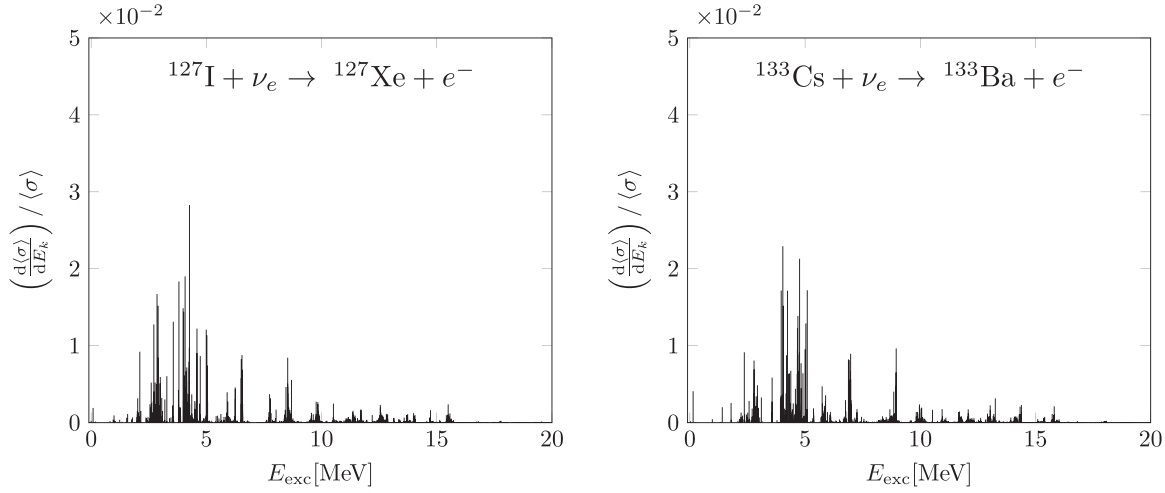

FIG. 7. Contributions to the total folded stopped-pion neutrino cross section from individual final nuclear states with energies E_{exc}, normalized to the total folded cross section.

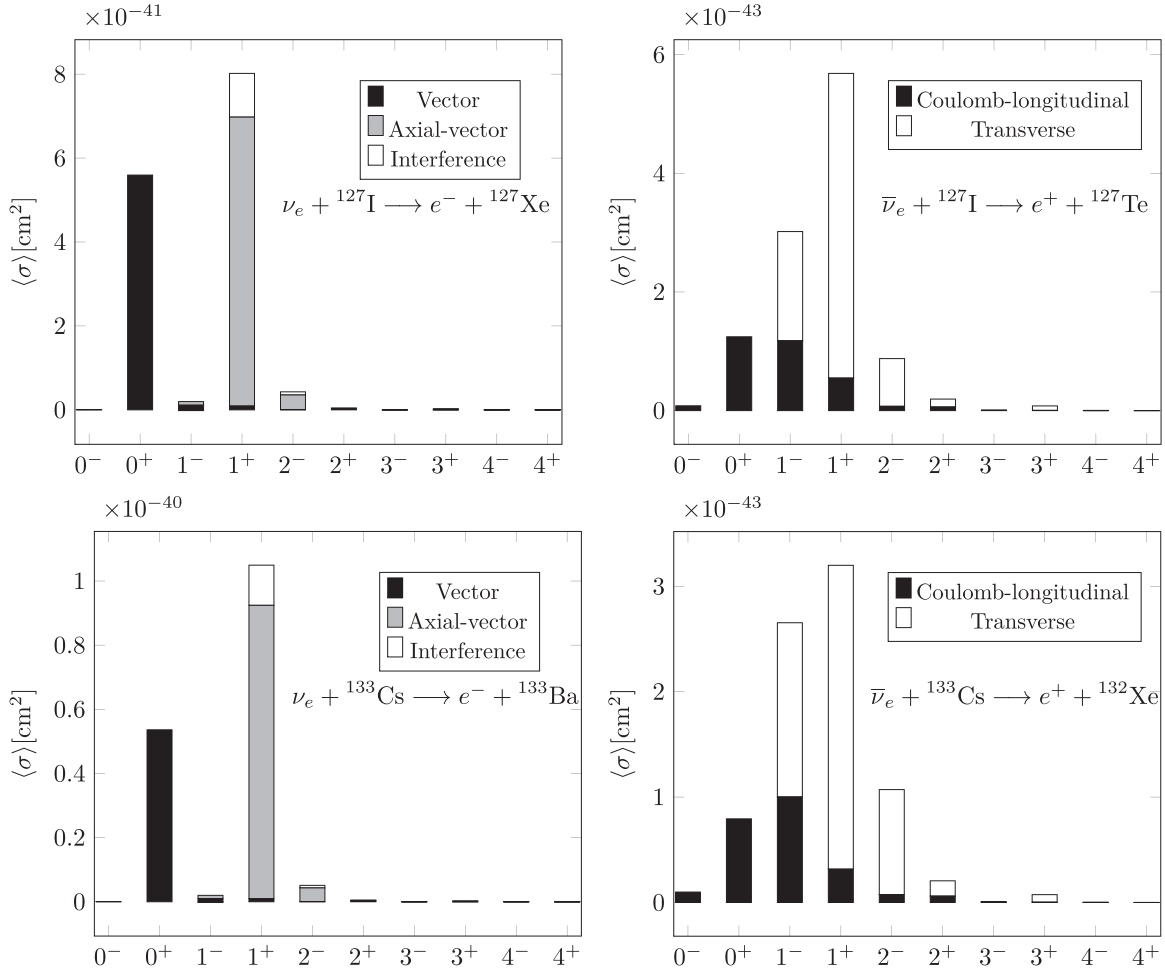

FIG. 8. Contributions of different multipoles to the total folded supernova-neutrino scattering cross section off ^{127}I (top) and ^{133}Cs (bottom) with $\alpha = 3$ for charged-current (anti)neutrinos on the (right) left. The parts with different tensorial character (vector, axial-vector, interference) for each individual multipole contribution for neutrinos and contributions from Coulomb-longitudinal and transverse parts for antineutrinos are also visualized. Higher multipoles not presented in the graphs have vanishingly small contributions.

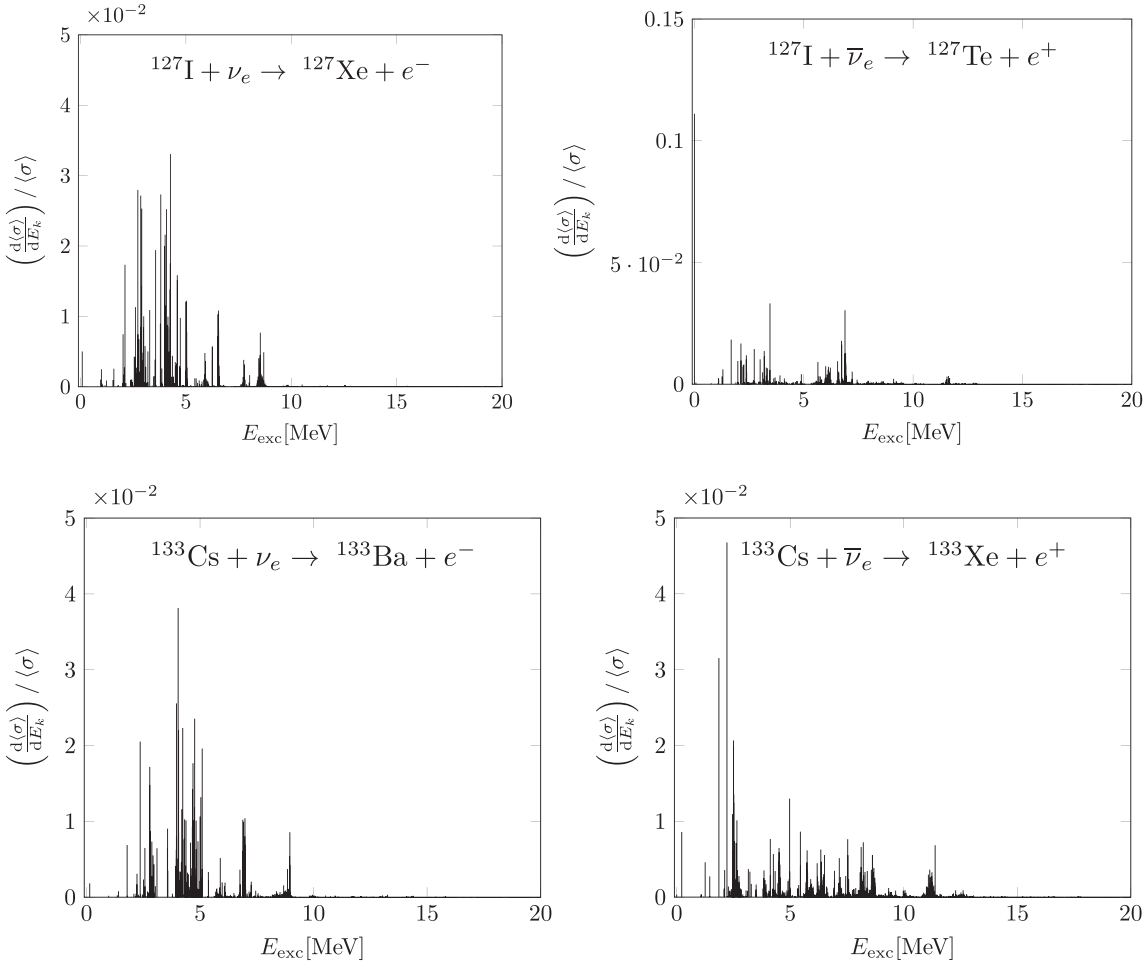

FIG. 9. Contributions to the total folded supernova neutrino cross section with $\alpha = 3$ from individual final nuclear states with energies E_{exc}, normalized to the total folded cross section.

this observation is even more pronounced in the charged-current results. For the neutral-current scattering there were some prominently contributing states that are reached via a forbidden transition, whereas in the contribution spectra for the charged-current results these type of states are fewer and their contributions smaller. To give an idea of this difference, the neutral-current electron scattering off ^{127}I using the reference nucleus ^{126}Te had several of these type of states that had contributions in the ∼1% range, compared to the charged-current scattering off ^{127}I for which the highest contributing state reached via a forbidden transition had a contribution of only 0.5%. As for the differences in the results between the two nuclei for the charged-current results, the different contribution spectra do share the general features of one another to a high degree, as was the case in our previous paper for the neutral-current scattering, as well.

C. Supernova-(anti)neutrino cross sections

The model we use for supernova (anti)neutrinos is based on a modified thermal Fermi-Dirac distribution [63,64]

$$p(E_\nu) = \frac{1}{T^3 F_2(\alpha)} \frac{E_\nu^2}{e^{E_\nu/T-\alpha}+1}, \tag{30}$$

where T is the effective (anti)neutrino temperature inside the supernova and $F_n(\alpha)$ the Fermi-Dirac integral

$$F_n(\alpha) = \int dx \frac{x^n}{1+e^{x-\alpha}}. \tag{31}$$

The degeneracy parameter α is introduced in order to better account for the damping of the high-energy tail of the spectrum. There is no consensus on what the exact value of the α parameter should be, and we have consequently computed the flux-averaged supernova (anti)neutrino scattering cross sections using two commonly used values for it, namely $\alpha = 0.0$ and $\alpha = 3.0$. These are the same values that were used in our previous work on neutral-current supernova (anti)neutrino scattering. The neutrino spectrum can be alternative parametrized in terms of the average neutrino energy $\langle E_\nu \rangle$, which is related to T and α by

$$\langle E_\nu \rangle = \frac{F_2(\alpha)}{F_3(\alpha)} T. \tag{32}$$

In this paper we have adopted the same commonly used values (in MeV) of $\langle E_{\nu_e} \rangle = 11.5$, $\langle E_{\overline{\nu}_e} \rangle = 13.6$, and $\langle E_{\nu_x/\overline{\nu}_x} \rangle = 16.3$, where we denote the combinations of both the μ and τ flavors by x.

The folded supernova (anti)neutrino scattering cross sections are presented in the same table as the previously discussed stopped-pion results, namely Table III. Most of the conclusions that can be drawn from them either follow directly from the unfolded results of Table II or from the same arguments as in the case of stopped-pion scattering; the neutrino scattering cross sections are larger than the corresponding antineutrino cross sections due to the threshold energies and the results for ^{133}Cs are larger than those of ^{127}I mainly because of the higher value of $g_{\mathrm{A,eff}}$ used in the computations for the latter. Another immediate observation that can be made is that a higher value for the degeneracy parameter corresponds to a lower effective neutrino temperature, and the results for $\alpha = 3$ are thus expectedly smaller than for $\alpha = 0$. Some of the multipole profiles and final-state contributions of charged-current supernova-neutrino scattering are illustrated in Figs. 8 and 9.

The main differences between the supernova-neutrino results and the corresponding stopped-pion results is that in the former the incoming lepton energy is notably smaller than in the latter. As a result, the supernova-neutrino scattering is even more dominated by allowed transition multipoles, as can be clearly seen in Fig. 8. The highly contributing final states in Fig. 9 are thus to an even greater degree composed of states that can be reached from the ground state of the mother nucleus through allowed transitions. In particular, the single most highly contributing state for the $\overline{\nu}_e + {}^{127}\mathrm{I}(5/2^+) \longrightarrow e^+ + {}^{127}\mathrm{Te}$ reaction is the $3/2^+$ ground state of the daughter nucleus, representing well over 10% of all the contributions to the reaction cross section. This reaction is the only one of the reactions listed in Eq. (2) to have an allowed ground-state-to-ground-state transition, which mostly explains the disproportionate contribution of this transition and why a similar effect is not observed in the contributions to other reactions.

IV. CONCLUSIONS

In this paper we have reviewed the theory of semileptonic nuclear processes. We have briefly discussed the theoretical formalism of the quasiparticle-based nuclear models QRPA and MQPM, and applied the latter of these to construct wave functions of the initial and final nuclear states for the charged-current (anti)neutrino scattering reactions off ^{127}I and ^{133}Cs. We have computed the scattering cross sections as functions of energy, and the total folded cross sections of stopped-pion and supernova neutrinos.

For both initial nuclei the neutrino scattering cross sections as functions of the energy of the incoming neutrino were found to be a few orders of magnitude larger than the corresponding antineutrino cross sections. This could be explained by the higher threshold energies of the latter reactions. Differences in the scattering results between the two nuclear targets were small, mostly arising from the different effective g_{A} values used for them. Folded cross sections were also computed for stopped-pion and supernova-(anti)neutrino spectra. The results for the former, in the case of ^{127}I, are in good agreement with the recent measurement of the COHERENT Collaboration.

The question of to what degree the quenching of g_{A} can explain the apparent discrepancy between the recent experimental result and the MARLEY estimate is more complicated and at this point inconclusive. While the computed inclusive cross section is in good agreement with experiment, the case of the exclusive cross section is more complicated and further research into this would be needed to arrive at a definite answer. Furthermore, it should be noted that an upper bound for $g_{\mathrm{A,eff}}$ extracted from the experiment was also reported in the same paper. This was obtained by comparing the upper 1σ uncertainty experimental result to the MARLEY estimate with the lower 1σ uncertainty for the input data [14]. As MARLEY does not currently incorporate forbidden transitions and employs the allowed approximation [15], experimentally measured Gamow-Teller strengths of ^{127}Xe were used as inputs [65]. These are also the source of the uncertainty in the MARLEY estimate. The resulting upper bound for $g_{\mathrm{A,eff}}$, which was $g_{\mathrm{A,eff}} \leqslant 0.97$ [14], does not contradict our choice of $g_{\mathrm{A,eff}}$ for ^{127}I.

ACKNOWLEDGMENTS

M.H. acknowledges financial support from the Väisälä Foundation of the Finnish Academy of Science and Letters.

[1] S. Fukuda, Y. Fukuda, T. Hayakawa, E. Ichihara, M. Ishitsuka, Y. Itow, T. Kajita, J. Kameda, K. Kaneyuki, S. Kasuga, K. Kobayashi, Y. Kobayashi, Y. Koshio, M. Miura, S. Moriyama, M. Nakahata, S. Nakayama, T. Namba, Y. Obayashi, A. Okada *et al.*, The Super-Kamiokande detector, Nucl. Instrum. Methods Phys. Res., Sect. A **501**, 418 (2003).

[2] N. Jelley, A. B. McDonald, and R. H. Robertson, The Sudbury neutrino observatory, Annu. Rev. Nucl. Part. Sci. **59**, 431 (2009).

[3] R. Abbasi, M. Ackermann, J. Adams, M. Ahlers, J. Ahrens, K. Andeen, J. Auffenberg, X. Bai, M. Baker, S. Barwick, R. Bay, J. Bazo Alba, K. Beattie, T. Becka, J. Becker, K.-H. Becker, P. Berghaus, D. Berley, E. Bernardini, D. Bertrand *et al.*, The IceCube data acquisition system: Signal capture, digitization, and timestamping, Nucl. Instrum. Methods Phys. Res., Sect. A **601**, 294 (2009).

[4] D. Akimov, P. An, C. Awe, P. S. Barbeau, P. Barton, B. Becker, V. Belov, A. Bolozdynya, A. Burenkov, B. Cabrera-Palmer, J. I. Collar, R. J. Cooper, R. L. Cooper, C. Cuesta, D. Dean, J. Detwiler, A. G. Dolgolenko, Y. Efremenko, S. R. Elliott, A. Etenko *et al.*, The COHERENT Experiment at the Spallation Neutron Source, arXiv:1509.08702v2.

[5] Y. Fukuda, T. Hayakawa, E. Ichihara, K. Inoue, K. Ishihara, H. Ishino, Y. Itow, T. Kajita, J. Kameda, S. Kasuga, K. Kobayashi, Y. Kobayashi, Y. Koshio, M. Miura, M. Nakahata, S. Nakayama, A. Okada, K. Okumura, N. Sakurai, M. Shiozawa *et al.*, Evidence for oscillation of atmospheric neutrinos, Phys. Rev. Lett. **81**, 1562 (1998).

[6] Q. R. Ahmad, R. C. Allen, T. C. Andersen, J. D. Anglin, G. Bühler, J. C. Barton, E. W. Beier, M. Bercovitch, J. Bigu, S. Biller, R. A. Black, I. Blevis, R. J. Boardman, J. Boger, E. Bonvin, M. G. Boulay, M. G. Bowler, T. J. Bowles, S. J. Brice, M. C. Browne *et al.*, Measurement of the rate of $\nu_e + d \rightarrow p + p + e^-$ interactions produced by ^{8}B solar neutrinos at the Sudbury Neutrino observatory, Phys. Rev. Lett. **87**, 071301 (2001).

[7] D. Akimov, J. B. Albert, P. An, C. Awe, P. S. Barbeau, B. Becker, V. Belov, A. Brown, A. Bolozdynya, B. Cabrera-Palmer, M. Cervantes, J. I. Collar, R. J. Cooper, R. L. Cooper, C. Cuesta, D. J. Dean, J. A. Detwiler, A. Eberhardt, Y. Efremenko, S. R. Elliott *et al.*, Observation of coherent elastic neutrino-nucleus scattering, Science **357**, 1123 (2017).

[8] F. An, G. An, Q. An, V. Antonelli, E. Baussan, J. Beacom, L. Bezrukov, S. Blyth, R. Brugnera, M. B. Avanzini, J. Busto, A. Cabrera, H. Cai, X. Cai, A. Cammi, G. Cao, J. Cao, Y. Chang, S. Chen, S. Chen *et al.*, Neutrino physics with JUNO, J. Phys. G **43**, 030401 (2016).

[9] A. Alekou, E. Baussan, N. B. Kraljevic, M. Blennow, M. Bogomilov, E. Bouquerel, A. Burgman, C. J. Carlile, J. Cederkall, P. Christiansen, M. Collins, E. C. Morales, P. Cupial, L. D. Alessi, H. Danared, J. P. A. M. de Andre, J. P. Delahaye, M. Dracos, I. Efthymiopoulos, T. Ekelof *et al.*, The european spallation source neutrino super beam, arXiv:2203.08803.

[10] I. Anghel, J. F. Beacom, M. Bergevin, C. Blanco, E. Catano-Mur, F. D. Lodovico, A. Elagin, H. Frisch, J. Griskevich, R. Hill, G. Jocher, T. Katori, F. Krennrich, J. Learned, M. Malek, R. Northrop, C. Pilcher, E. Ramberg, J. Repond, R. Sacco *et al.*, Letter of intent: The accelerator neutrino neutron interaction experiment (ANNIE), arXiv:1504.01480.

[11] J. A. Formaggio and G. P. Zeller, From eV to EeV: Neutrino cross sections across energy scales, Rev. Mod. Phys. **84**, 1307 (2012).

[12] R. Maschuw, B. Armbruster, G. Drexlin, V. Eberhard, K. Eitel, H. Gemmeke, T. Jannakos, M. Kleifges, J. Kleinfeller, C. Oehler *et al.*, From eV to EeV: Neutrino cross sections across energy scales, Prog. Part. Nucl. Phys. **40**, 183 (1998).

[13] P. An, C. Awe, P. S. Barbeau, B. Becker, S. W. Belling, V. Belov, I. Bernardi, C. Bock, A. Bolozdynya, R. Bouabid, A. Brown, J. Browning, B. Cabrera-Palmer, M. Cervantes, E. Conley, J. Daughhetee, J. Detwiler, K. Ding, M. R. Durand, Y. Efremenko *et al.*, Measurement of ^{nat}Pb(ν_e, Xn) production with a stopped-pion neutrino source, Phys. Rev. D **108**, 072001 (2023).

[14] P. An, C. Awe, P. S. Barbeau, B. Becker, V. Belov, I. Bernardi, C. Bock, A. Bolozdynya, R. Bouabid, A. Brown, J. Browning, B. Cabrera-Palmer, M. Cervantes, E. Conley, J. Daughhetee, J. Detwiler, K. Ding, M. R. Durand, Y. Efremenko, S. R. Elliott, L. Fabris, M. Febbraro, A. G. Rosso, A. Galindo-Uribarri, A. C. Germer, M. P. Green, J. Hakenmueller, M. R. Heath, S. Hedges, M. Hughes *et al.*, Measurement of the inclusive electron-neutrino charged-current cross section on ^{127}I with the COHERENT NaIνE detector, Phys. Rev. Lett. **131**, 221801 (2023).

[15] S. Gardiner, Simulating low-energy neutrino interactions with MARLEY, Comput. Phys. Commun. **269**, 108123 (2021).

[16] H. Lee, H. Bhang, J. Choi, I. Hahn, D. He, M. Hwang, H. Kim, S. Kim, S. Kim, S. Kim, T. Kim, Y. Kim, J. Kwak, Y. Kwon, J. Lee, J. Lee, J. Lee, M. Lee, J. Li, S. Myung *et al.*, First limit on WIMP cross section with low background CsI(Tl) crystal detector, Phys. Lett. B **633**, 201 (2006).

[17] E. Barbosa de Souza, J. Cherwinka, A. Cole, A. C. Ezeribe, D. Grant, F. Halzen, K. M. Heeger, L. Hsu, A. J. F. Hubbard, J. H. Jo, A. Karle, M. Kauer, V. A. Kudryavtsev, K. E. Lim, C. Macdonald, R. H. Maruyama, F. Mouton, S. M. Paling, W. Pettus, Z. P. Pierpoint *et al.*, First search for a dark matter annual modulation signal with NaI(Tl) in the Southern Hemisphere by DM-Ice17, Phys. Rev. D **95**, 032006 (2017).

[18] K. Fushimi, H. Ejiri, R. Hazama, H. Ikeda, K. Imagawa, K. Inoue, G. Kanzaki, A. Kozlov, R. Orito, T. Shima, Y. Takemoto, Y. Teraoka, S. Umehara, K. Yasuda, and S. Yoshida, Dark matter search project PICO-LON, J. Phys.: Conf. Ser. **718**, 042022 (2016).

[19] J. Amaré, S. Cebrián, I. Coarasa, C. Cuesta, E. García, M. Martínez, M. A. Oliván, Y. Ortigoza, A. O. de Solórzano, J. Puimedón, A. Salinas, M. L. Sarsa, P. Villar, and J. A. Villar, First results on dark matter annual modulation from the anais-112 experiment, Phys. Rev. Lett. **123**, 031301 (2019).

[20] W. C. Haxton, Radiochemical neutrino detection via ^{127}I(ν_e, e^-)^{127}Xe, Phys. Rev. Lett. **60**, 768 (1988).

[21] J. Engel, S. Pittel, and P. Vogel, Responses of ^{127}I to solar neutrinos, Phys. Rev. Lett. **67**, 426 (1991).

[22] J. Engel, S. Pittel, and P. Vogel, Capture of solar and higher-energy neutrinos by ^{127}I, Phys. Rev. C **50**, 1702 (1994).

[23] T. S. Kosmas and E. Oset, Charged current neutrino-nucleus reaction cross sections at intermediate energies, Phys. Rev. C **53**, 1409 (1996).

[24] S. Mintz and M. Pourkaviani, Inclusive neutrino reactions in ^{127}I, Nucl. Phys. A **584**, 665 (1995).

[25] M. Athar, S. Ahmad, and S. Singh, Neutrino nucleus cross sections for low energy neutrinos at SNS facilities, Nucl. Phys. A **764**, 551 (2006).

[26] J. R. Distel, B. T. Cleveland, K. Lande, C. K. Lee, P. S. Wildenhain, G. E. Allen, and R. L. Burman, Measurement of the cross section for the reaction ^{127}I(ν_e, e^-) ^{127}Xe$_{\text{bound states}}$ with neutrinos from the decay of stopped muons, Phys. Rev. C **68**, 054613 (2003).

[27] B. Goulard and H. Primakoff, Nuclear structure effects in "elastic" neutrino-induced reactions, Phys. Rev. **135**, B1139 (1964).

[28] J. Bell and C. H. L. Smith, Quasielastic neutrino-nucleus interactions, Nucl. Phys. B **28**, 317 (1971).

[29] T. K. Gaisser and J. S. O'Connell, Interactions of atmospheric neutrinos in nuclei at low energy, Phys. Rev. D **34**, 822 (1986).

[30] T. Kuramoto, M. Fukugita, Y. Kohyama, and K. Kubodera, Neutrino-induced reaction cross sections at intermediate energies for chlorine and water detectors, Nucl. Phys. A **512**, 711 (1990).

[31] Y. Lutostansky, G. Koroteev, N. Klochkova, A. Osipenko, V. Tikhonov, and A. Fazliakhmetov, New capabilities of an iodine detector for solar neutrinos, JETP Lett. **111**, 603 (2020).

[32] Y. Lutostansky, G. Koroteev, N. Klochkova, A. Osipenko, V. Tikhonov, and A. Fazliakhmetov, Effect of high-lying resonances on cross sections for solar-neutrino capture by ^{127}I nuclei, Phys. At. Nucl. **83**, 391 (2020).

[33] Y. Lutostansky, A. Fazliakhmetov, G. Koroteev, N. Klochkova, A. Lutostansky, A. Osipenko, and V. Tikhonov, New prospects for iodine detector and Solar neutrinos registration, Phys. Lett. B **826**, 136905 (2022).

[34] R. Blin-Stoyle, Renormalization of the axial-vector coupling constant in β-decays, Nucl. Phys. A **254**, 353 (1975).
[35] F. Khanna, I. Towner, and H. Lee, Quenching of axial-vector coupling constant in the β-decay of finite nuclei, Nucl. Phys. A **305**, 349 (1978).
[36] J. Suhonen, Value of the axial-vector coupling strength in β and $\beta\beta$ decays: A review, Front. Phys. **5**, 55 (2017).
[37] M. Wang, W. Huang, F. Kondev, G. Audi, and S. Naimi, The AME 2020 atomic mass evaluation (II). Tables, graphs and references, Chin. Phys. C **45**, 030003 (2021).
[38] E. Tiesinga, P. Mohr, D. Newell, and B. Taylor, *2018 CODATA Recommended Values of the Fundamental Constants of Physics and Chemistry*, Special Publication (NIST SP) No. 959 (National Institute of Standards and Technology, Washington, 2019).
[39] H. Ejiri, J. Suhonen, and K. Zuber, Neutrino-nuclear responses for astro-neutrinos, single beta decays and double beta decays, Phys. Rep. **797**, 1 (2019).
[40] T. Donnelly and R. Peccei, Neutral current effects in nuclei, Phys. Rep. **50**, 1 (1979).
[41] J. Walecka, *Theoretical Nuclear and Subnuclear Physics* (Imperial College, London, 2004).
[42] E. Ydrefors, K. Balasi, J. Suhonen, and T. Kosmas, in *Neutrinos: Properties, Sources and Detection*, edited by J. Greene (Nova Science, New York, 2011), pp. 151–175.
[43] J. Engel, Approximate treatment of lepton distortion in charged-current neutrino scattering from nuclei, Phys. Rev. C **57**, 2004 (1998).
[44] A. Fetter and J. Walecka, *Quantum Theory of Many-Particle Systems* (McGraw-Hill, New York, 1971).
[45] J. Bjorken and S. Drell, *Relativistic Quantum Mechanics* (McGraw-Hill, New York, 1965).
[46] M. Gell-Mann and M. Lévy, The axial vector current in beta deacy, Nuovo Cimento **16**, 705 (1960).
[47] B. Märkisch, H. Mest, H. Saul, X. Wang, H. Abele, D. Dubbers, M. Klopf, A. Petoukhov, C. Roick, T. Soldner, and D. Werder, Measurement of the weak axial-vector coupling constant in the decay of free neutrons using a pulsed cold neutron beam, Phys. Rev. Lett. **122**, 242501 (2019).
[48] W. Haxton and E. Henley, *Symmetries and Fundamental Interactions in Nuclei* (World Scientific, Singapore, 1995).
[49] J. Suhonen, *From Nucleons to Nucleus: Concepts of Microscopic Nuclear Theory* (Springer-Verlag, Berlin, 2007).
[50] J. Engel and J. Menéndez, Status and future of nuclear matrix elements for neutrino less double beta decay: A review, Rep. Prog. Phys. **80**, 046301 (2017).
[51] M. Agostini, G. Benato, J. A. Detwiler, J. Menéndez, and F. Vissani, Toward the discovery of matter creation with neutrinoless Double-Beta decay, Rev. Mod. Phys. **95**, 025002 (2023).
[52] P. Pirinen and J. Suhonen, Systematic approach to β and $2\nu\beta\beta$ decays of mass $A = 100$–136 nuclei, Phys. Rev. C **91**, 054309 (2015).
[53] H. Ejiri, N. Soukouti, and J. Suhonen, Spin-dipole nuclear matrix elements for double beta decays and astro-neutrinos, Phys. Lett. B **729**, 27 (2014).
[54] J. Kostensalo and J. Suhonen, Spin-multipole nuclear matrix elements in the *pn* quasiparticle random-phase approximation: Implications for β and $\beta\beta$ half-lives, Phys. Rev. C **95**, 014322 (2017).
[55] J. Toivonen and J. Suhonen, Microscopic quasiparticle-phonon description of odd-A Xe isotopes, J. Phys. G **21**, 1491 (1995).
[56] J. Toivanen and J. Suhonen, Microscopic quasiparticle-phonon description of odd-mass $^{127-133}$Xe isotopes and their β decay, Phys. Rev. C **57**, 1237 (1998).
[57] A. Bohr and B. Mottelson, *Nuclear Structure* (Benjamin, New York, 1969), Vol. 1.
[58] J. Suhonen, A. Faessler, T. Taigel, and T. Tomoda, Suppression of the β^+-decays if ^{148}Dy, ^{150}Er and ^{152}Yb, Phys. Lett. B **202**, 174 (1988).
[59] J. Suhonen, T. Taigel, and A. Faessler, pnQPRA calculation of the β^+/EC quenching for several neutron-deficient nuclei in mass regions $A = 94$–110 and $A = 146$–156, Nucl. Phys. A **486**, 91 (1988).
[60] A. Hashizume, Nuclear data sheets for A = 127, Nucl. Data Sheets **112**, 1647 (2011).
[61] Y. Khazov, A. Rodionov, and F. Kondev, Nuclear data sheets for A = 133, Nucl. Data Sheets **112**, 855 (2011).
[62] M. Hellgren and J. Suhonen, Neutral-current supernova neutrino-nucleus scattering off ^{127}I and ^{133}Cs, Phys. Rev. C **106**, 025808 (2022).
[63] H.-T. Janka and W. Hillebrandt, Monte Carlo simulations on neutrino transport in type II supernovae, Astron. Astrophys. Suppl. Ser. **78**, 375 (1989).
[64] M. Keil, G. Raffelt, and H.-T. Janka, Monte Carlo study of supernova neutrino spectra formation, Astrophys. J. **590**, 971 (2003).
[65] M. Palarczyk, J. Rapaport, C. Hautala, D. L. Prout, C. D. Goodman, I. van Heerden, J. Sowinski, G. Savopulos, X. Yang, H. M. Sages, R. Howes, R. Carr, M. Islam, E. Sugarbaker, D. C. Cooper, K. Lande, B. Luther, and T. N. Taddeucci, Measurement of Gamow-Teller strength for ^{127}I as a solar neutrino detector, Phys. Rev. C **59**, 500 (1999).